RESEARCH ARTICLE

A double-network hydrogel for the dynamic compression of the lumbar nerve root

Hui Li[1,#], **Hua Meng**[1,#], **Yan-Yu Yang**[2,3], **Jia-Xi Huang**[1], **Yong-Jie Chen**[1], **Fei Yang**[2,*], **Jia-Zhi Yan**[1,*]
1 Department of Orthopedic Surgery, Beijing Tiantan Hospital, Capital Medical University, Beijing, China
2 Institute of Chemistry, Chinese Academy of Science, Beijing, China
3 Zhengzhou University, Zhengzhou, Henan Province, China

Funding: *This work was supported by the High Levels of Health Technical Personnel in Beijing Health System of China, No. 2013-3-050 (to JZY).*

Graphical Abstract

An experimental model for dynamic compression of the lumbar nerve root produced by double-network (DN) hydrogel in rats

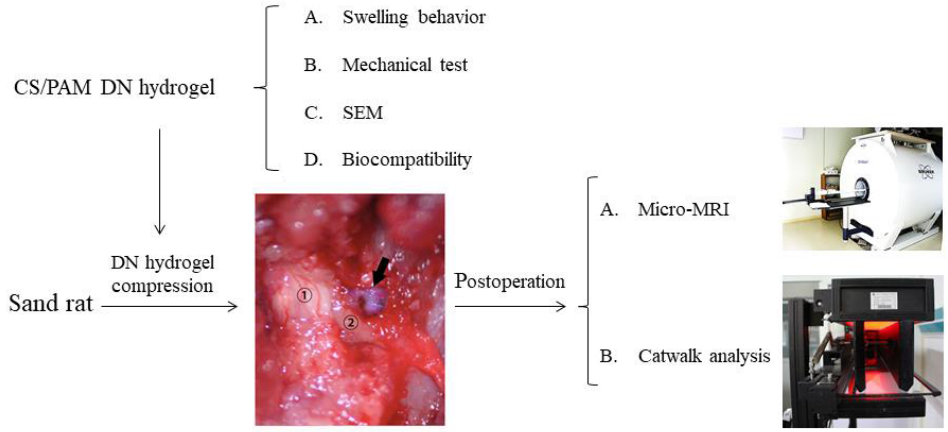

Correspondence to:
Jia-Zhi Yan, PhD, beijingtiantan@163.com;
Fei Yang, fyang@iccas.ac.cn.

#Both authors contributed equally to this paper.

orcid:
0000-0001-7404-4688 (Jia-Zhi Yan)

doi: *10.4103/1673-5374.276361*

Received: *July 23, 2019*
Peer review started: *July 26, 2019*
Accepted: *August 19, 2019*
Published online: *February 28, 2020*

Abstract

Current animal models of nerve root compression due to lumbar disc herniation only assess the mechanical compression of nerve roots and the inflammatory response. Moreover, the pressure applied in these models is static, meaning that the nerve root cannot be dynamically compressed. This is very different from the pathogenesis of lumbar disc herniation. In this study, a chitosan/polyacrylamide double-network hydrogel was prepared by a simple two-step method. The swelling ratio of the double-network hydrogel increased with prolonged time, reaching 140. The compressive strength and compressive modulus of the hydrogel reached 53.6 and 0.34 MPa, respectively. Scanning electron microscopy revealed the hydrogel's crosslinked structure with many interconnecting pores. An MTT assay demonstrated that the number of viable cells in contact with the hydrogel extracts did not significantly change relative to the control surface. Thus, the hydrogel had good biocompatibility. Finally, the double-network hydrogel was used to compress the L4 nerve root of male sand rats to simulate lumbar disc herniation nerve root compression. The hydrogel remained in its original position after compression, and swelled with increasing time. Edema appeared around the nerve root and disappeared 3 weeks after operation. This chitosan/polyacrylamide double-network hydrogel has potential as a new implant material for animal models of lumbar nerve root compression. All animal experiments were approved by the Animal Ethics Committee of Neurosurgical Institute of Beijing, Capital Medical University, China (approval No. 201601006) on July 29, 2016.

Key Words: *chitosan; double-network hydrogel; dynamic compression; lumbar disc herniation; micro-MRI; nerve root; peripheral neuropathic pain; polyacrylamide*

Chinese Library Classification No. *R458; R741; R318.08*

Introduction

The chronic compression of lumbar spinal nerve roots by intervertebral disc herniation is a leading cause of lower back pain and sciatica in humans. The symptoms of lower back pain and sciatica (also classified as chronic peripheral neuropathic pain) are chronic spontaneous pain and/or hypersensitivity to normally painful stimulation and normally non-painful stimulation, as well as the dysesthesias and/or parasthesias (Bogduk, 2009). Eventually, patients may undergo operation for lumbar disc herniation to relieve the pain. However, removal of herniated disc materials does not relieve symptoms in many patients, and pain recurrence after lumbar discectomy has been shown to occur (Wankhade et al., 2016; Suri et al., 2017).

Animal models of lumbar disc herniation may help to understand the complex pathophysiological mechanisms associated with lumbar radicular pain. During the past decades, many animal models have been established to mimic lumbar neuropathic pain. These models have been produced according to two main factors: inflammation and compression. Inflammation models include the application of an autologous lumbar intervertebral disc (Kato et al., 2015; Handa et al., 2016; Yan et al., 2016) or an allografted coccygeal intervertebral disc (Suzuki et al., 2009; Kim et al., 2011; Sasaki et al., 2011; Cho et al., 2013) to the rat nerve root without mechanical compression as a model of non-compressive intervertebral disc herniation. These experiments result in painful radiculopathy by releasing proinflammatory cytokines from the nucleus pulposus. Compression models have been established using suture ligation (Winkelstein et al., 2001, 2002; Winkelstein and DeLeo, 2004), silicon tube (Xue et al., 2014), an L-shaped stainless steel rod (Sasaki et al., 2010; Fan et al., 2011), an ameroid constrictor (Cornefjord et al., 1997), metal clips (Igarashi et al., 2005), and inflatable balloons (Olmarker et al., 1990, 1991). The use of these models results in endoneurial edema and Wallerian degeneration of the nerve root. Moreover, both types of radiculopathy model can eventually induce a neuroinflammatory response and neuronoglial apoptosis; decreases in nerve conduction velocities; and the onset of mechanical hyperalgesia and thermal hyperalgesia (Olmarker et al., 1991; Winkelstein et al., 2002; Winkelstein and DeLeo, 2004; Igarashi et al., 2005; Fan et al., 2011; Kim et al., 2011; Yan et al., 2016). However, all chronic spinal nerve root compression models have been applied with the aim of establishing steady compression of the spinal nerve. In the clinic, the histopathological change of lumber intervertebral disc herniation can be divided into different types, which can result in different mechanical compression and adhesion with the lumbar nerve root (Yang and Lu, 2017). The most common scenario is the gradual compression of the spinal nerve by the herniated disc rather than static, chronic compression (Miyagi et al., 2012).

Hydrogels — soft materials with a three-dimensional, crosslinked network structure — are promising materials for drug delivery, actuation, sensing and tissue engineering (Liu and Blesch, 2018; Wang et al., 2019). Double-network (DN) hydrogels are composed of two asymmetric networks with differing properties. Synergism between the two networks endows DN hydrogels with outstanding mechanical performance (Duan et al., 2015; Yang et al., 2016).

In the present study, we prepared a chitosan/polyacrylamide (CS/PAM) DN hydrogel, consisting of a CS microcrystalline network and a PAM covalent network. We applied the DN hydrogel in an animal model for chronic and dynamic lumbar nerve root compression.

Materials and Methods

Hydrogel fabrication procedure

As shown in **Figure 1**, the CS/PAM DN hydrogel was prepared via a two-step method, as reported in our previous work (Yang et al., 2016). Briefly, acrylamide monomer (1.8 g; Sigma-Aldrich, St. Louis, MO, USA), short-chain chitosan (1.0 g, degree of deacetylation > 90%, viscosity of 45 mPa·s for 1% (w/v) solution; Shandong Jinhu Company, Linyi, China), 2-hydroxy-4′-(2-hydroxyethoxy)-2-methylpropiophenone photoinitiator (Irgacure 2959, 57.6 mg, 1 mol% relative to the acrylamide monomer; Sigma-Aldrich) and N, N′--methylene-bis-acrylamide crosslinker (0.03 mol% relative to acrylamide; Sigma-Aldrich) were added into 10 mL of H_2O. After heating at 60°C and violent vibration, the mixture became a transparent solvent, which was then poured into a customized glass mold to prepare a cylindrical CS/PAM composite hydrogel under ultraviolet radiation (150 W). The composite hydrogel was immersed into 1 M NaOH for 20 minutes to produce the CS crystalline network and yield the CS/PAM DN hydrogel. The CS/PAM DN hydrogel was used after removing unreacted acrylamide monomer by thorough dialysis (**Figure 2**).

Hydrogel swelling

The CS/PAM DN hydrogel samples were weighed (W_0; XB10201, Shanghai Precision Instrument Co., Shanghai, China) and then soaked into a large amount of water at 25°C, which was replaced daily. After a predetermined time, the swollen hydrogel samples were taken out and weighed (W_s) again. The swelling ratio (g/g) of the hydrogel was calculated as $(W_s - W_0)/W_0$.

Mechanical tests

All mechanical tests were performed with an Instron Model 5567 machine (Instron, Norwood, MA, USA) in air at room temperature and 30% humidity. The cylindrical hydrogel samples (height = 15 mm, diameter = 12 mm) were used for compressive tests at a rate of 5 mm/minute. The entire loading process was finished in less than five minutes to avoid redistribution of the solvent inside the gel. The force and displacement were recorded continuously throughout the experiment.

Scanning electron microscopy

Scanning electron microscopy analysis was performed to evaluate the microstructure of the CS/PAM DN hydrogel. Hydrogel samples were freeze-dried using a lyophilizer and coated with a conductive Pt film before being used for field-emission scanning electron microscopy (JSM-6700; JEOL Ltd., Tokyo, Japan) at a voltage of 5 kV.

In vitro experiments

A model was designed to evaluate the swelling behavior of the hydrogel and the resulting compression conditions (**Figure 3**). A bungee was used to simulate a nerve compressed by the hydrogel. The bungee passed through the hydrogel donut, and medical-grade silica was used to fix the hydrogel. The whole system was immersed in a sufficient amount of water to make the hydrogel swell and exert pressure on the bungee.

Biocompatibility analysis

Animals

Two healthy male sand rats (3-days old) and 20 male sand rats (200–250 g, 3-month old) were purchased from Peking Weitonglihua Laboratory Animal Center (Beijing, China)

(license No. SXCK(Jing)2007-0001). All animal experiments were approved by the Animal Ethics Committee of the Neurosurgical Institute of Beijing, Capital Medical University, China (approval No. 201601006) on July 29, 2016.

Isolation and culture of Schwann cells

Two 3-day-old rats were used for testing the biocompatibility and biosafety of the hydrogel. After the rats were anesthetized, the bilateral sciatic nerves were exposed and transected at the level of the mid-thigh hindlimb, and then the nerves were washed in PBS solution. Using an operating microscope (ASOM-3B; Chengdu Corder Optics & Electronics Co., Chengdu, China), the epineurium was dissected with microsurgical instruments, and grown in a culture medium, containing Dulbecco's Modified Eagle's medium (Corning, New York, NJ, USA), 5% fetal calf serum (Gibco, Grand Island, NY, USA), and 1% antibiotic (penicillin and streptomycin, Sigma-Aldrich) for 24 hours at 37°C and 5% CO_2 until confluency.

Cell viability assessment

CS/PAM DN hydrogels were washed four times in sterile PBS and were then exposed to UV radiation for two periods of 15 minutes to inactivate any microorganisms present. Finally, the hydrogels were immersed in cell culture medium for 24 hours before cell seeding. After a 24-hour incubation period, the culture medium was removed and dilutions (100%, 75%, 50%, and 25%) of the 100% extracts were added to cell plate wells for 24 hours in the culture medium. Schwann cells were seeded at a density of 1×10^5 cells/well in a 96-well plate. Cells were incubated at 37°C in an atmosphere of 5% CO_2 in air. Cell growth, cell adhesion, and visual proliferation were evaluated using an optical inverted fluorescence microscope (IX53; Olympus, Tokyo, Japan). Cell viability was assessed using 3-(4,5-dimethylthiazol-2-yl)-2,5-diphenyltetrazolium bromide (MTT) assay. The optical density at 492 nm was measured using a microplate reader. The cell viability (%) was calculated followed the formula [A] test/[A] control × 100, where [A] test and [A] control are the optical density values of the wells (with the hydrogel) and control wells (without hydrogel), respectively.

***In vivo* experiments**

Surgical procedure

The 20 male sand rats were randomly assigned to the model group (n = 15) or the control group (n = 5). The sterilized surgical procedures were intraperitoneally anesthetized with sodium pentobarbital (40 mg/kg). Using an operating microscope, a right L4 hemi-laminectomy was performed to expose the right L4 nerve roots. The diameter of the L4 nerve root was measured at 2 mm proximal to the dorsal root ganglia. The L4 nerve roots were compressed using the DN hydrogels (n = 15); the control group underwent no surgical procedure (n = 5). The length of the DN hydrogel cube was equal to the diameter of the L4 nerve root and was implanted 2 mm proximal to the dorsal root ganglia. The initial length of the hydrogel cube was determined using an eyepiece micrometer under the microscope. The paraspinal muscle was carefully closed to form a relatively closed space around the hydrogel and the incision was closed in layers. To prevent infection, all animals in the model group received intramuscular injections of 800,000 units of penicillin on the day of surgery and on each of the following 3 days (Xue et al., 2014).

Micro-MRI evaluation

Scanning was performed using a 7.0-T micro-MRI (BioClinScan Animal MRI System, Siemens, Billerica, USA) with a maximum gradient strength of 290 mT/m (**Figure 4**). All rats were intraperitoneally anesthetized using sodium pentobarbital (40 mg/kg) before scanning. Rats were placed on the examining bed in the prone position. A series of sagittal T2-weighted scans was obtained to ascertain the swelling process of the hydrogel.

Micro-MRI scanning was performed in five rats each from the control and model groups at 1, 2, and 3 weeks post-operation. The control rats were sacrificed at 7 days after micro-MRI scanning. The diameter of the right L4 nerve root compressed by the hydrogel in the model group was calculated in the T2 transverse MRI scans. The water content (%) of the hydrogel in the model group post-operation was calculated after weighing the hydrogel on an electronic balance (Shanghai Huachao Industrial Company, Shanghai, China). The L4 nerve roots and hydrogels in the model and control groups were resected for macroscopic analysis. The water content was independently measured three times per condition. The experiment and calculations were performed by two independent, blinded observers. The investigator who analyzed the data was blinded to the animal status.

Gait analysis

A CatWalk XT system (Noldus Information Technology, Wageningen, the Netherlands) was used to analyze the gait pre- and post-operation. In brief, the rats were placed on a glass plate located in a darkened room and allowed to walk freely in the system. The entire course of walking was recorded by an automatic video camera in the system. The data were acquired and analyzed by the CatWalk software. All rats walked three times on the glass plate pre- and post-operation. The footprints and gait dynamics of all rats were recorded three times and analyzed using the CatWalk system.

Statistical analysis

All data are expressed as the mean ± standard deviation (SD). For *in vitro* studies, each experiment was tested three times to determine the reproducibility. One-way analysis of variance, followed by a Game–Howell *post hoc* test, was performed to evaluate significant differences using SPSS 19.0 software (SPSS Inc., Chicago, IL, USA). A value of $P \leq 0.05$ was considered statistically significant.

Results

Swelling behavior

High water absorption is an essential property of a hydrogel. The swelling behavior of our hydrogel is displayed in **Figure 2A** and **B**. With increasing immersion time, the swelling ratio (g/g) increased, reaching an equilibrium swelling ratio of 140 after 10 days.

Mechanical performance

A high mechanical strength of the hydrogel is important for dynamic compression on the lumbar nerve root (Olmarker et al., 1990, 1991; Xue et al., 2014). The compressive property of the CS/PAM hydrogel was estimated, as shown in **Figure 2C**. The hydrogel remained intact during compression, even at a strain of 96%. The compressive strength reached 53.6 MPa. As calculated from the enlarged plot in **Figure 2D**, the compressive modulus of the hydrogel reached a high value of 0.34 MPa, which allows it to exert pressure on the lumbar nerve root.

Microstructure analysis

The microstructure of the CS/PAM DN hydrogel is shown in **Figure 5**. Scanning electron microscopy images revealed a typical crosslinked structure of the hydrogel with a large number of interconnecting pores.

***In vitro* simulation of hydrogel swelling**

The *in vitro* model, which consisted of a bungee, hydrogel, and medical-grade silica, was immersed in water to evaluate whether the hydrogel exerts pressure on the bungee. As shown in **Figure 3B**, the bungee was free in the hydrogel donut before soaking in water. However, after immersion in water for 1 hour, the bungee was fixed by the hydrogel owing to water absorption and swelling of the hydrogel. After an additional 5 hours, the hydrogel absorbed a large amount of water and swelled significantly. The restriction of the silica facilitated compression of the central bungee by the hydrogel. These experiments demonstrated that the hydrogel should be able to exert pressure on the lumbar nerve root.

Biocompatibility

It is necessary to evaluate the toxicity and biocompatibility of biomaterials before *in vivo* studies (Venkatesan et al., 2014; Teimouri et al., 2017). As observed in **Figure 6**, the viability of rat Schwann cells in all extract dilutions exceeded 90%, and remained the same regardless of the concentration of the extract ($P > 0.05$). Ocular inspection of the Schwann cells under a fluorescence microscope revealed that the cell morphology in each extract dilution was round or oval, and there were no changes in apoptotic contraction or collapse (**Figure 7**).

The right L4 nerve roots extended from the upper lumbar spinal cord to the narrow L4 lumbar intervertebral foramen, almost filling the space of the intervertebral foramen. The normal L4 nerve root was white and clear, and the blood vessels on the surface of the nerves were distributed equality (**Figure 8A**). The diameter of the L4 right nerve root 2 mm proximal to the dorsal root ganglia was 0.92 ± 0.08 mm. The length of the DN hydrogel cube was equal to the diameter of the L4 nerve roots. Compression of the nerve root by the hydrogel resulted in edema and hyperemia, which diffused along the nerve root at 1 week post-operation (**Figure 8B** and **C**). The minimal inflammatory response may be due to the operation injury. Three weeks following the surgery, the edema and hyperemia disappeared, and scar tissue formed (**Figure 8D**).

In the XT version of the CatWalk gait analysis system, two dimensions of the rats' footprints over a limited time period were reconstructed to show the dynamic change from toe on to toe off (**Figure 9B**). At 1 and 2 weeks post-injury, there were significantly different footprints of the right hind paws compared with pre-operation, indicated by the decreases in intensity (**Figure 9A** and **B**). The mean stand (i.e., the duration that the rat's paw remains in contact with the plate) for the right hind paw pre-operation was significantly longer than at 4 weeks after surgery ($P = 0.004$). The mean stand for the right hind paws at 2 weeks post-injury was significantly higher than pre-operation, and 3 and 4 weeks after surgery ($P = 0.004$, $P = 0.041$, $P = 0.001$, respectively). The mean stand for the right hind paw 3 weeks post-injury was significantly higher than 4 weeks after surgery ($P = 0.02$; **Figure 9C**). There was no significant difference in the mean stand for the right front paw between the repeated interventions ($P > 0.05$; **Figure 9C**).

Dynamic changes of hydrogel compression of nerve roots

T2 Micro-MRI scans showed the normal dorsal nerve root and surrounding tissue. The signal intensity of the spinal cord and lumbar spinal nerve appeared white in the scans. A pair of spinal dorsal nerves were dissociated from the spinal cord and passed through the intervertebral foramen (**Figure 10A**). In the model group, 1 week after surgery, hematoma formed around the wound. The hydrogel, which appeared black in the scans, was located on the surface of the L4 nerve root (**Figure 10B**). Two weeks after surgery, the hematoma around the wound disappeared. The hydrogel had a mixed signal intensity, and increased in size as it absorbed the surrounding water (**Figure 10C**). Three weeks after surgery, the wound had recovered. At this time point, the hydrogel also showed a mixed signal intensity, its size was larger than at 2 weeks post-surgery, and its location remained unchanged (**Figure 10D**).

The water content of the CS/PAM DN hydrogel was 0.194 ± 0.082% at 1 week post-operation, 0.413 ± 0.045% at 2 weeks post-operation, and 0.530 ± 0.039% at 3 weeks post-operation. The water content at 3 weeks post-operation was significantly higher at 1 and 2 weeks ($P < 0.05$ and $P = 0.008$, respectively); the water content at 2 weeks was significantly higher than at 1 week post-operation ($P < 0.05$).

Discussion

Lumbar disc herniation and stenosis of the lumbar intervertebral foramen are major causes of lower back pain. Although our understanding of the pathological mechanisms of disc herniation and lumbar spinal stenosis related to radiculopathy has developed over the past decades, key gaps in knowledge remain. Although there is a distinction between the pain-related behaviors of humans and animals, most of our understanding of radicular pain is based on animal models. An ideal animal model that mimics the lumbar neuropathic pain should comply with the following recommendations: (1) the etiology of the pain symptoms should be similar to that in clinical situations; (2) pain-related behaviors should resemble the specific symptoms of radiculopathy and be measured; (3) the animal model should be propitious to the study of the basic pathophysiologic mechanisms; and

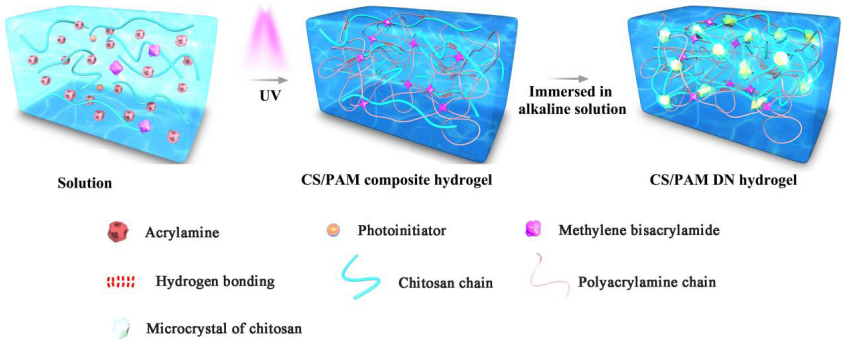

Figure 1 Preparation of the CS/PAM DN hydrogel.
The CS/PAM DN hydrogel was prepared via a two-step method. CS and PAM were first mixed to construct a CS/PAM composite hydrogel via UV radiation. The composite hydrogel was then converted into a CS/PAM DN hydrogel by immersion in an alkaline solution. CS: Chitosan; DN: double-network; PAM: polyacrylamide.

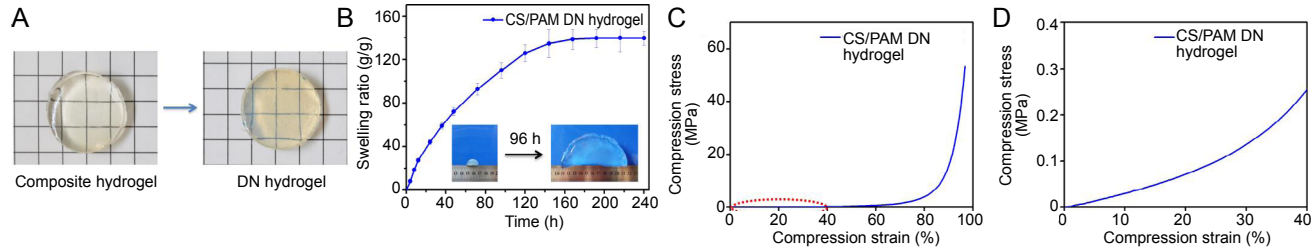

Figure 2 Characterization of the hydrogels.
(A) Photographs of the CS/PAM composite hydrogel and DN hydrogel. (B) Swelling behavior of the CS/PAM DN hydrogel. (C, D) Compressive curves of the CS/PAM DN hydrogel. The maximal strain was set at 96%. The curve in panel D represents the part marked in panel C. CS: Chitosan; DN: double-network; PAM: polyacrylamide.

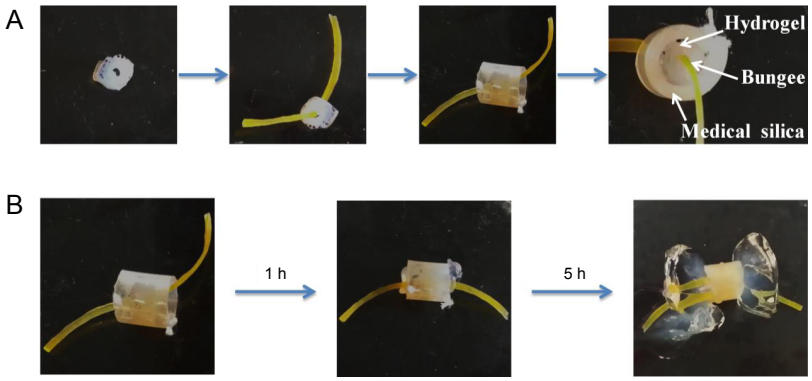

Figure 3 *In vitro* simulation experiment mimicking the *in vivo* swelling behavior of the hydrogel and the resulting compression of the surrounding material.
(A) Preparation of the model: A bungee passed through the hydrogel donut, which was fixed with medical-grade silica. The whole system was immersed in a sufficient amount of water to make the hydrogel swell and exert pressure on the bungee. (B) Results: With increasing immersion time, the swelling ratio of the CS/PAM DN hydrogel increased, resulting in the dynamic compression of the bungee.

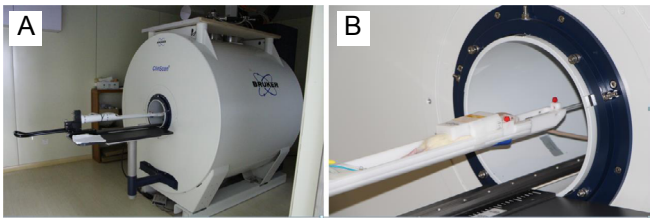

Figure 4 Fixation of the radiofrequency coil and animal handling before 7.0-T micro-MRI scanning.
(A) Photograph of the high-resolution micro-MRI scanner. (B) Photograph of the rat cassette of the system. MRI: Magnetic resonance imaging.

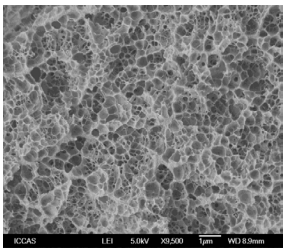

Figure 5 Scanning electron microscopy images of the CS/PAM DN hydrogel.
The CS/PAM DN hydrogel exhibits a dense network structure and uniformly small pores. CS: Chitosan; DN: double-network; PAM: polyacrylamide.

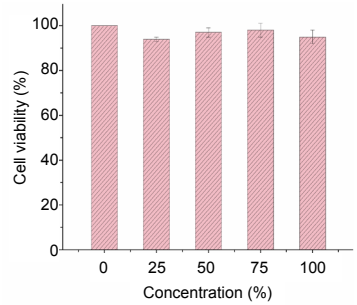

Figure 6 Biocompatibility of the CS/PAM DN hydrogel.
Optical density of formazan obtained by MTT assays of rat Schwann cells in contact with hydrogels after 24 hours of growth (control: 0%, Schwann cells grown on polystyrene multi-well plates without the hydrogel). All data are expressed as the mean ± SD (n = 5). P > 0.05 for each extract dilution compared with the control group (0.94 ± 0.01, 0.97 ± 0.02, 0.98 ± 0.03 and 0.95 ± 0.03, corresponding respectively to 25%, 50%, 75% and 100% extract dilutions). The experiment was performed in triplicate to determine the reproducibility. CS: Chitosan; DN: double-network; MTT: 3-(4,5-dimethylthiazol-2-yl)-2,5-diphenyltetrazolium bromide; PAM: polyacrylamide; SD: standard deviation.

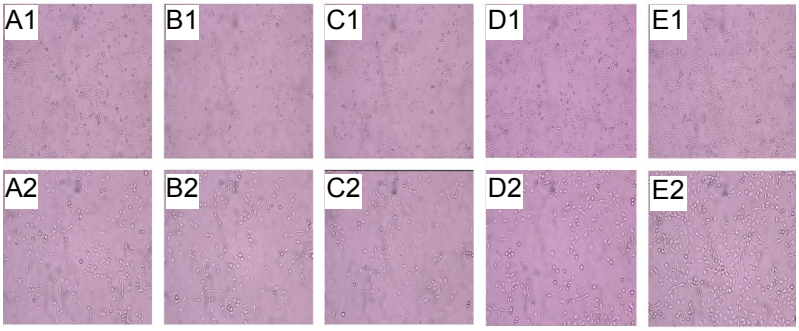

Figure 7 Morphology of Schwann cells seeded on hydrogel extracts at different dilutions.
In contrast with the control group (E, Schwann cells grown on polystyrene multi-well plates without hydrogel), the cell morphology in 25% (A), 50% (B), 75% (C) and 100% (D) extract dilutions is round or oval, and there is no change in cell apoptosis, cell pyknosis, or cell disintegration. Scale bars: 200 μm for the upper panels (1) and 400 μm for the lower panels (2) . The experiment was performed in triplicate to determine the reproducibility.

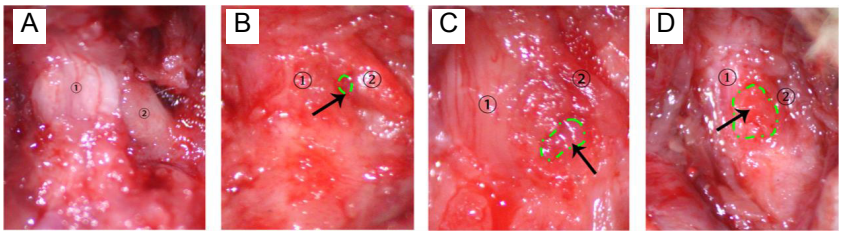

Figure 8 Anatomical images of the animal model.
(A) Normal right nerve root, which is white and clear. (B) L4 nerve root 7 days after surgery: the nerve root was compressed by the DN hydrogel, which caused edema and hyperemia. (C) L4 nerve root 14 days after surgery: the edema and hyperemia diffused along the nerve root, and the position of the hydrogel was unchanged. (D) L4 nerve root 21 days after surgery: the edema and hyperemia disappeared, and the size of the hydrogel increased. The black arrows indicate the position of CS/PAM DN hydrogel; the green circles indicate the size change of the hydrogel with prolonged time. ① : Cauda equine; ② : L4 nerve root. CS: Chitosan; DN: double-network; PAM: polyacrylamide.

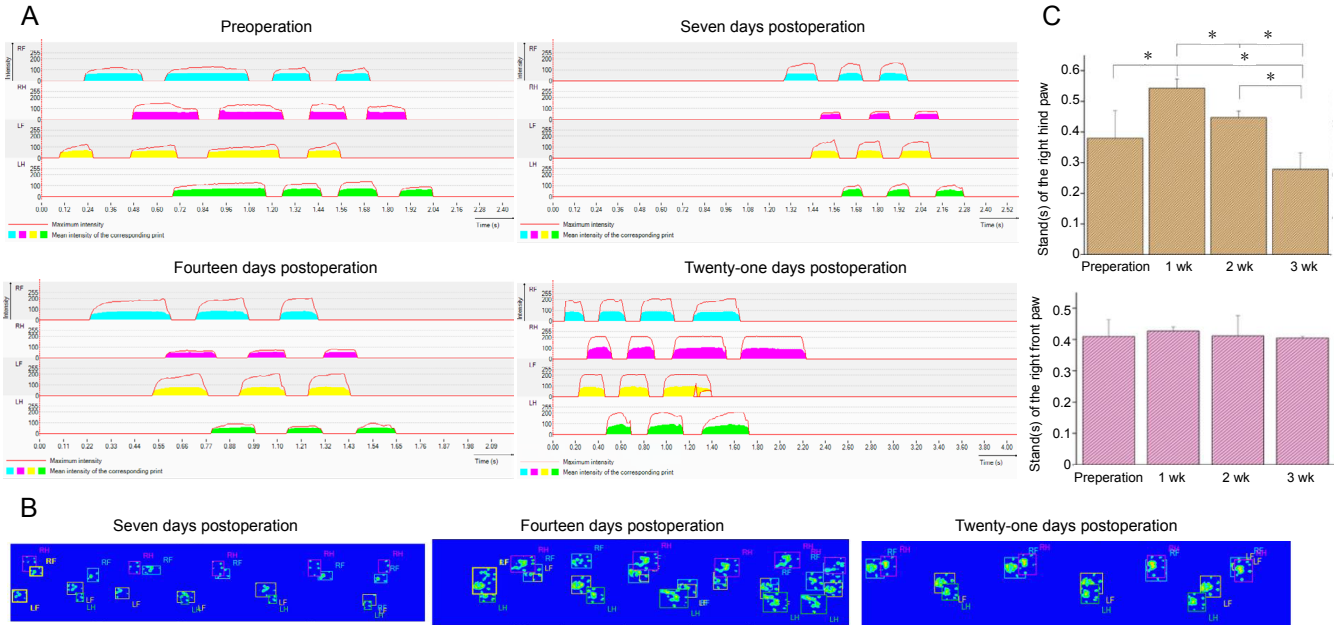

Figure 9 CatWalk XT analysis after a right L4 hemi-laminectomy on sand rats with the CS/PAM DN hydrogel.
(A) Intensity of the footprints of the rats: Purple shows the footprints of the right hind foot (the compression side); light blue shows the footprints of the right front foot. (B) Illustration of the footprints in the model groups at different time points: Red shows the footprints of the right hind foot (the compression side); green shows the footprints of the right front foot (normal side). (C) The stand of right hind paws and front paws, which indicates the duration of contact of a paw with the glass plate measured in seconds. All data are expressed as the mean ± SD. $*P < 0.05$ (one-way analysis of variance followed by Game-Howell *post hoc* test). LF: Left front paw; LH: left hind paw; RF: right front paw; RH: right hind paw. CS: Chitosan; DN: double-network; PAM: polyacrylamide; SD: standard deviation.

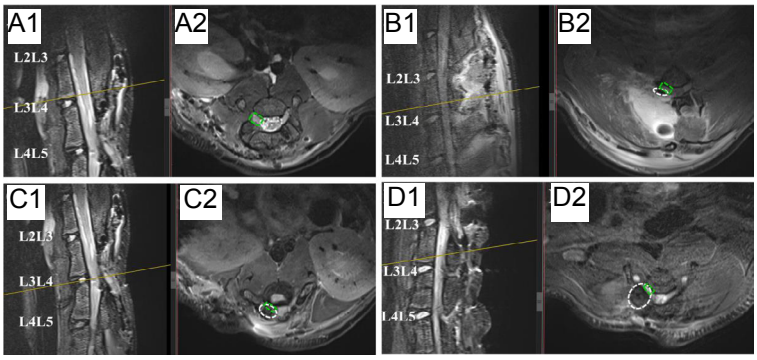

Figure 10 Sagittal and axial micro-MR images of the animal model.
(A) T2 MRI scans of the normal L4 nerve roots in the control group and the surrounding tissues. (B–D) T2 MRI scans of the L4 nerve roots and the DN hydrogel 1 week after surgery. The green dotted line indicates the L4 nerve roots and the white dotted line indicates the DN hydrogel. The size of the CS/PAM DN hydrogel increases and dynamically compresses the L4 nerve roots with prolonged time. CS: Chitosan; DN: double-network; MRI: magnetic resonance imaging; PAM: polyacrylamide. A1, B1, C1 and D1: sagittal micro-MR images; A2, B2, C2 and D2: axial micro-MR images.

(4) the experimental methods should be simple, repeatable, and have a high rate of success (Mogil, 2009).

Mechanical deformation of the lumbar spinal nerve to mimic lumbar radiculopathies has been studied extensively during the past decades. Moreover, dozens of animal models of neuropathic pain have been established. To study the mechanism of lumbar radiculopathies, it is important to select both a suitable animal model and an appropriate compressive substance. As mentioned earlier, mechanical deformation has been induced by either suture ligation (Winkelstein et al., 2001, 2002; Winkelstein and DeLeo, 2004), or using a silicon tube (Xue et al., 2014), an L-shaped stainless steel rod (Sasaki et al., 2010; Fan et al., 2011), an ameroid constrictor (Cornefjord et al., 1997), metal clips (Igarashi et al., 2005), or inflatable balloons (Olmarker et al., 1990, 1991), with or without the exposure to the nucleus pulposus. In the clinic, herniated discs cause degeneration of the spinal nerve; this is exacerbated as the herniated nucleus pulposus becomes more severe. During intervertebral disc herniation, the lumbar spinal nerve roots are dynamically compressed by the herniated disc.

The animal models used to date suffer the following inherent limitations in light of the discussion above: (1) the mechanical pressure produced by compressive substances is static, chronic compression not dynamic; (2) implants such as inflatable balloons are difficult to fix around the cauda equine and must be implanted into large animals, which may limit their clinical utility; (3) the biocompatibility of silicon tubes is untested; and (4) implantation of an L-shaped stainless steel rod into the lumbar intervertebral foramen damages the nerve root (as we found that the lumbar nerve roots almost filled in the space of the intervertebral foramen). Thus, it is necessary to develop a new animal model that closely mimics the pathogenic process of lumbar disc herniation and spinal stenosis to improve our understanding of these diseases, and to test the efficacy of new regenerative strategies.

Our new composite DN hydrogel may be used as a compressive material to closely mimic the mechanism of lumbar neuropathic pain. To be suitable in a dynamic and chronic animal model, the material must have appropriate swelling properties and mechanical strength. First, it is necessary for the hydrogel to absorb a large amount of water in the model of lumbar disc herniation to produce gradually increasing compression. *In vitro*, the CS/PAM DN hydrogel absorbed water and swelled quickly, with a remarkable swelling ratio (g/g) that reached 140. The continuous water absorption and excellent swelling behavior indicated that the DN hydrogel was superhydrophilic. In particular, the microcrystalline CS in the DN hydrogel provided the excellent stability and high swelling ratio.

High mechanical strength of hydrogel is also necessary for producing dynamic compression. The hydrogel embraces the nerve roots, and should gradually compress them after absorbing water. Thus, the mechanical strength should increase upon swelling. The composite hydrogel was generally too brittle and weak to bear force, especially upon swelling in water. However, the CS/PAM DN hydrogel exhibited the required compressive performance owing to its two anisotropic networks with contrasting properties. The high density of short CS chains formed a firm CS physical network, which combined with the elastic covalent PAM network. The DN hydrogel was very strong, with a compressive strength of 53.6 MPa and a compressive modulus of 0.34 MPa. We attribute the high compressive strength to the bonding between the CS and PAM networks, which may improve their ductility and toughness, and form dense network structures with high cross-link density.

The excellent compressive and swelling performance of our DN hydrogel allowed it to dynamically exert pressure on the lumbar nerve root. To evaluate the swelling pressure of the hydrogel, a simulated model experiment was carried out after water absorption. The central bungee initially moved freely, but was then tightly fixed by the swollen hydrogel. Unexpectedly, the swollen hydrogel still exerted a compressive force on the central bungee. The results of this experiment confirmed the suitability of the CS/PAM DN hydrogel for compression of the lumbar nerve root.

For the *in vitro* MTT assays, the optical density values were proportional to the number of viable cells and no significant differences relative to the control group were observed. Furthermore, observation of the cellular morphology revealed the absence of cell apoptosis, cell pyknosis, and changes in cell disintegration for cells cultured in the hydrogel extracts. These results suggest that the DN hydrogels are biocompatible.

The use of micro-MRI to study the swelling process and position of the hydrogels post-operation was advantageous because: (1) it is non-invasive in contrast with micro-CT and histological staining; (2) the animals could be scanned under general anesthesia without sacrifice; (3) it is a simple operating process (Li et al., 2017). The micro-MRI investigation revealed that the position of the DN hydrogel did not change during swelling; the size of the hydrogel increased in situ during the entire 3-week observation period; and that the DN hydrogels retained the structural integrity.

CatWalk XT is a new research tool for tracking the footprints and gait dynamics in rodent models. This has been applied to various models of pain and to evaluate the motor function, such as models of spinal cord injury, inflammatory pain and mechanical allodynia, and lumbar disease (Kameda et al., 2017; Fukui et al., 2018). The assessment of gait and locomotion in rodent models is important in conditions that affect the central and peripheral nervous systems. In the present study, we observed changes of the footprints and stand of the right hind paw in the rats of the model group using the CatWalk XT system. These changes reflect pain-related behavior, as has been observed in other neuropathic pain animal models. In contrast with other implants, the DN hydrogel supplies dynamically increasing compressive pressure to the lumbar nerve roots, resulting in the progressive exacerbation of symptoms, which closely mimics lumbar neuropathic pain. Similar to the *in vitro* experiments, we believe that mechanical strength of the DN hydrogel increases by absorbing the surrounding water *in vivo*. On the basis of these results, we believe this hydrogel could be a suitable implant material for animal models of lumbar nerve root compression in the future.

There are some limitations of this study. Firstly, we did not carry out behavioral testing, electrophysiological recordings, or histopathologic analysis before and after surgery. These methods should be applied in further research. Secondly, the size of the hydrogel used in rats is very small; the accuracy and reliability of the data could be further increased by using large-sized animals. Thirdly, the biocompatibility study was only conducted for 7 days. These should be conducted over a longer period of time to assess possible long-term cytotoxicity of these implants.

Conclusions

We applied a mechanically strong CS/PAM DN hydrogel with high water absorption to exert gradually increasing pressure on the lumbar nerve root, mimicking the formation of lumbar disc herniation. The DN hydrogel gradually swelled *in vivo* and dynamically compressed the lumbar nerve root. Therefore, this is a suitable implant material for new animal models of lumbar nerve root compression.

Acknowledgments: *The authors thank the members of their laboratories for making this study possible.*
Author contributions: *Study concept and design: JZY, FY; experimental implementation: HL, YYY, HM, JXH and YJC. Data analysis and paper writing: HL and YYY. All authors approved the final version of the paper.*
Conflicts of interest: *There were no conflicts of interest in this experiment.*
Financial support: *This study was supported by the High Levels of Health Technical Personnel in Beijing Health System of China, No. 2013-3-050 (to JZY).*
Institutional review board statement: *All animal experiments were approved by the Animal Ethics Committee of Neurosurgical Institute of Beijing, Capital Medical University, China (approval No. 201601006) on July 29, 2016.*
Copyright license agreement: *The Copyright License Agreement has been signed by all authors before publication.*
Data sharing statement: *Datasets analyzed during the current study are available from the corresponding author on reasonable request.*
Plagiarism check: *Checked twice by iThenticate.*
Peer review: *Externally peer reviewed.*

Open peer reviewers: *Michele R. Colonna, Universita degli Studi di Messina, Italy; Ming-Chao Huang, Taipei Veterans General Hospital, China.*

References

Bogduk N (2009) On the definitions and physiology of back pain, referred pain, and radicular pain. Pain 147:17-19.
Cho HK, Cho YW, Kim EH, Sluijter ME, Hwang SJ, Ahn SH (2013) Changes in pain behavior and glial activation in the spinal dorsal horn after pulsed radiofrequency current administration to the dorsal root ganglion in a rat model of lumbar disc herniation: laboratory investigation. J Neurosurg Spine 19:256-263.
Cornefjord M, Sato K, Olmarker K, Rydevik B, Nordborg C (1997) A model for chronic nerve root compression studies. Presentation of a porcine model for controlled, slow-onset compression with analyses of anatomic aspects, compression onset rate, and morphologic and neurophysiologic effects. Spine (Phila Pa 1976) 22:946-957.
Duan J, Liang X, Cao Y, Wang S, Zhang L (2015) High strength chitosan hydrogels with biocompatibility via new avenue based on constructing nanofibrous architecture. Macromolecules 48:2706-2714.
Fan N, Donnelly DF, LaMotte RH (2011) Chronic compression of mouse dorsal root ganglion alters voltage-gated sodium and potassium currents in medium-sized dorsal root ganglion neurons. J Neurophysiol 106:3067-3072.
Fukui D, Kawakami M, Matsumoto T, Naiki M (2018) Stress enhances gait disturbance induced by lumbar disc degeneration in rat. Eur Spine J 27:205-213.
Handa J, Sekiguchi M, Krupkova O, Konno SI (2016) The effect of serotonin-noradrenaline reuptake inhibitor duloxetine on the intervertebral disk-related radiculopathy in rats. Eur Spine J 25:877-887.
Igarashi T, Yabuki S, Kikuchi S, Myers RR (2005) Effect of acute nerve root compression on endoneurial fluid pressure and blood flow in rat dorsal root ganglia. J Orthop Res 23:420-424.
Kameda T, Kaneuchi Y, Sekiguchi M, Konno SI (2017) Measurement of mechanical withdrawal thresholds and gait analysis using the CatWalk method in a nucleus pulposus-applied rodent model. J Exp Orthop 4:31-31.
Kato K, Sekiguchi M, Kikuchi Si, Konno Si (2015) The effect of a 5-HT2A receptor antagonist on pain-related behavior, endogenous 5-hydroxytryptamine production, and the expression 5-HT2A receptors in dorsal root ganglia in a rat lumbar disc herniation model. Spine (Phila Pa 1976) 40:357-362.
Kim SJ, Park SM, Cho YW, Jung YJ, Lee DG, Jang SH, Park HW, Hwang SJ, Ahn SH (2011) Changes in expression of mRNA for interleukin-8 and effects of interleukin-8 receptor inhibitor in the spinal dorsal horn in a rat model of lumbar disc herniation. Spine (Phila Pa 1976) 36:2139-2146.
Li H, Yan JZ, Chen YJ, Kang WB, Huang JX (2017) Non-invasive quantification of age-related changes in the vertebral endplate in rats using in vivo DCE-MRI. J Orthop Surg Res 12:169-169.
Liu S, Blesch A (2018) Targeted tissue engineering: hydrogels with linear capillary channels for axonal regeneration after spinal cord injury. Neural Regen Res 13:641-642.
Miyagi M, Ishikawa T, Kamoda H, Suzuki M, Murakami K, Shibayama M, Orita S, Eguchi Y, Arai G, Sakuma Y, Kubota G, Oikawa Y, Ozawa T, Aoki Y, Toyone T, Takahashi K, Inoue G, Kawakami M, Ohtori S (2012) ISSLS prize winner: disc dynamic compression in rats produces long-lasting increases in inflammatory mediators in discs and induces long-lasting nerve injury and regeneration of the afferent fibers innervating discs: a pathomechanism for chronic discogenic low back pain. Spine (Phila Pa 1976) 37:1810-1818.
Mogil JS (2009) Animal models of pain: progress and challenges. Nat Rev Neurosci 10:283-294.
Olmarker K, Rydevik B, Hansson T, Holm S (1990) Compression-induced changes of the nutritional supply to the porcine cauda equina. J Spinal Disord 3:25-29.
Olmarker K, Holm S, Rosenqvist AL, Rydevik B (1991) Experimental nerve root compression. A model of acute, graded compression of the porcine cauda equina and an analysis of neural and vascular anatomy. Spine (Phila Pa 1976) 16:61-69.
Sasaki N, Sekiguchi M, Kikuchi SI, Konno SI (2010) Anti-nociceptive effect of bovine milk-derived lactoferrin in a rat lumbar disc herniation model. Spine (Phila Pa 1976) 35:1663-1667.
Sasaki N, Sekiguchi M, Shishido H, Kikuchi SI, Yabuki S, Konno SI (2011) A comparison of pain-related behavior following local application of nucleus pulposus and/or mechanical compression on the dorsal root ganglion. Fukushima J Med Sci 57:46-53.
Suri P, Pearson AM, Zhao W, Lurie JD, Scherer EA, Morgan TS, Weinstein JN (2017) Pain recurrence after discectomy for symptomatic lumbar disc herniation. Spine (Phila Pa 1976) 42:755-763.
Suzuki M, Inoue G, Gemba T, Watanabe T, Ito T, Koshi T, Yamauchi K, Yamashita M, Orita S, Eguchi Y, Ochiai N, Kishida S, Takaso M, Aoki Y, Takahashi K, Ohtori S (2009) Nuclear factor-kappa B decoy suppresses nerve injury and improves mechanical allodynia and thermal hyperalgesia in a rat lumbar disc herniation model. Eur Spine J 18:1001-1007.
Teimouri A, Azadi M, Shams Ghahfarokhi Z, Razavizadeh R (2017) Preparation and characterization of novel β-chitin/nanodiopside/nanohydroxyapatite composite scaffolds for tissue engineering applications. J Biomater Sci Polym Ed 28:1-14.
Venkatesan J, Bhatnagar I, Kim SK (2014) Chitosan-alginate biocomposite containing fucoidan for bone tissue engineering. Mar Drugs 12:300-316.
Wang T, Zeng LN, Zhu Z, Wang YH, Ding L, Luo WB, Zhang XM, He ZW, Wu HF (2019) Effect of lentiviral vector-mediated overexpression of hypoxia-inducible factor 1 alpha delivered by pluronic F-127 hydrogel on brachial plexus avulsion in rats. Neural Regen Res 14:1069-1078.
Wankhade UG, Umashankar MK, Reddy BSJ (2016) Functional outcome of lumbar discectomy by fenestration technique in lumbar disc prolapse - return to work and relief of pain. J Clin Diagn Res 10:RC09-RC13.
Winkelstein BA, DeLeo JA (2004) Mechanical thresholds for initiation and persistence of pain following nerve root injury: mechanical and chemical contributions at injury. J Biomech Eng 126:258-263.
Winkelstein BA, Weinstein JN, DeLeo JA (2002) The role of mechanical deformation in lumbar radiculopathy: an in vivo model. Spine (Phila Pa 1976) 27:27-33.
Winkelstein BA, Rutkowski MD, Weinstein JN, DeLeo JA (2001) Quantification of neural tissue injury in a rat radiculopathy model: comparison of local deformation, behavioral outcomes, and spinal cytokine mRNA for two surgeons. J Neurosci Methods 111:49-57.
Xue F, Wei Y, Chen Y, Wang Y, Gao L (2014) A rat model for chronic spinal nerve root compression. Eur Spine J 23:435-446.
Yan J, Zou K, Liu X, Hu S, Wang Q, Miao X, Zhu HY, Zhou Y, Xu GY (2016) Hyperexcitability and sensitization of sodium channels of dorsal root ganglion neurons in a rat model of lumber disc herniation. Eur Spine J 25:177-185.
Yang L, Lu HH (2017) Value of a new pathological classification of lumbar intervertebral disc herniation based on transforaminal endoscopic observations. Exp Ther Med 13:1859-1867.
Yang Y, Wang X, Yang F, Shen H, Wu D (2016) A universal soaking strategy to convert composite hydrogels into extremely tough and rapidly recoverable double-network hydrogels. Adv Mater 28:7178-7184.

P-Reviewers: Colonna MR, Huang MC; C-Editor: Zhao M; S-Editors: Wang J, Li CH; L-Editors: Brotchie A, Raye W, Qiu Y, Song LP; T-Editor: Jia Y